CU Journal of Non-Linear Fluid Mechanics
Vol. 02, No. 01, 2026
https://doi.org/10.11615/cujnlfm.02104-6

Retention of Axially Input Arsenic Contaminants in a Heterogeneous Groundwater System under Sorption Isotherm Models

R Iyer Aiswarya[a] and S Nagouda Smita *[a, b]

[a] Department of Mathematics, CHRIST (Deemed to be University), Bangalore, 560029, INDIA.

[b] Centre for Mathematical Needs, CHRIST (Deemed to be University), Bangalore, 560029, INDIA.

Abstract

The presence of arsenic contaminants in groundwater poses a risk to the surrounding ecosystem. The retention of contaminants in the soil medium leads to soil degradation and affects vegetation, with the risk of desorption. This research focuses on the retention strength of arsenic contaminant onto the soil medium under different sorption models (Henry, Freundlich, Langmuir and Tóth). It presents a two-dimensional numerical model for contaminant transport in groundwater, governed by the advection-dispersion equation (ADE). A concentration-dependent retardation factor is considered for the sorption models to introduce nonlinearity into the system. An Alternating Direction Implicit (ADI) scheme, combined with the Thomas algorithm, is employed to ensure numerical stability and computational efficiency for long-term simulations. The numerical results demonstrate that nonlinear sorption significantly attenuates contaminant migration and modifies arsenic plume evolution compared to non-sorbing cases. The spatial concentration maps of arsenic contaminants, compared with unit retardation, reveal substantial accumulation within the soil matrix. This highlights the significance of accounting for nonlinear sorption effects in the realistic transport and fate of groundwater contamination. A study on a soil medium revealed that the amount of arsenic retained in the medium is directly proportional to the soil's Al/Fe content, offering insights for environmental studies and understanding the harmful effects of arsenic retention. The research is aligned with SDG 3 (Good Health and Well-being), SDG 6 (Clean Water and Sanitation), and SDG 14 (Life Below Water).

Keywords: Arsenic transport; Sorption isotherm; Heterogeneous groundwater system; Sorbed-phase concentration; Soil retention .

1 Introduction

Groundwater, being a critical freshwater source for domestic, agricultural and industrial purposes worldwide, is increasingly threatened by contamination. Contamination from natural and anthropogenic sources, including agricultural runoff, industrial effluents, and urban discharge, alters the hydrochemical equilibrium of groundwater [1]. This poses serious ecological and public health risks, necessitating appropriate monitoring and remediation strategies [2]. The attenuation and transport of contaminants in groundwater are influenced by interactions among hydrogeological, chemical, and biological factors; therefore, accounting for these factors is a practical necessity for accurate prediction of contaminant transport [3].

* smita.nagouda@christuniversity.in

Heavy metals, particularly like arsenic, are persistent in the soil matrix due to their bioaccumulative nature [4]. Recent studies have highlighted elevated levels of arsenic in groundwater systems across South and Southeast Asia, posing a higher risk of chronic exposure to the health risks associated with arsenic consumption [5]. Although arsenic is naturally present in sediments and bedrock, anthropogenic sources such as mining and industrial effluents exacerbate the mobilisation of the pollutant in groundwater and soil matrix [6]. In an aqueous environment, arsenic exists as arsenite (As(III)) under reducing conditions and as arsenate (As(V)) under oxidising conditions, and each oxidation state exhibits different mobility, toxicity, and behaviour under sorption models [7], [8]. Increased exposure to heavy metals like arsenic through groundwater is associated with severe health conditions such as cancers, cardiovascular diseases, and neurotoxicity [9]. Recent geochemical studies reveal that heterogeneity in sediment composition, redox conditions, and hydrological gradients significantly alters the mobilisation and attenuation of arsenic [10]. Nghiem et al. [11] showed that aluminium(Al) and/or iron(Fe) rich aquifer systems have accelerated arsenic content, and sulfate-reducing conditions show accelerated arsenic release under sulfatereducing conditions. Similarly, Wang et al. [12] highlighted that coastal aquifers affected by seawater intrusion exhibit complex zonation patterns for trace metals such as arsenic.

Experimental and field studies demonstrated that arsenic transport is susceptible to mineral composition and redox conditions [13]. Engineered sorbents with higher sorption capacities and greater potential for remediation, such as biochar and iron-based clay materials, have been investigated for the retention of the species [14]. Heterogeneous aquifers provide a medium for modified adsorption due to the presence of competing ions, which necessitated the inclusion of competitive sorption mechanisms [7]. Contaminant transport of any species in groundwater is governed by three mechanisms: advection, dispersion and diffusion [15]. The interaction of the species with soil particles or other species present in the system is governed by sorption characteristics and reaction decay, as well as geochemical reactions that significantly alter plume evolution [16]. Adsorption of species depends on soil texture, and the species are classified using sorption isotherms such as Henry, Langmuir, and Freundlich, along with their extended models, depending on the applicability to the medium [17].

Mathematical modelling is an indispensable tool for understanding species migration patterns in groundwater systems, particularly when experimental and field data cannot be obtained by conventional means. The mathematical representation of contaminants in groundwater is through the advection-dispersion equation (ADE), which accounts for the combined effects of hydrogeochemical factors in the system [18]. Since the equations are generally multidimensional, obtaining an analytical solution for realistic groundwater settings is inefficient. Numerical methods provide effective solutions to address system complexities through discretisation. Among the available finite-difference methods in the literature [19], the Peaceman-Rachford-Alternating Direction Implicit (PR-ADI) scheme has been widely adopted to decompose the ADE into successive one-dimensional implicit systems, thereby improving the numerical efficiency of the resulting solutions [20].

Despite considerable advancements in the field, investigations in existing studies are limited to homogeneous aquifers and individual sorption isotherms. Investigations evaluating linear and nonlinear sorption models in a heterogeneous groundwater system for arsenic species within a realistic framework are limited. Furthermore, computationally efficient numerical frameworks for accurately simulating concentration-dependent retention of arsenic species in the domain remain an active area of research. To address the limitations, the study aims to examine arsenic transport in a two-dimensional groundwater system, accounting for heterogeneity using an asymptotic formulation.

In this study, we define a two-dimensional ADI-based finite-difference framework that integrates multiple sorption isotherm models to simulate arsenic transport in a saturated heterogeneous aquifer. Incorporating multiple adsorption isotherm models enables a systematic comparison of aqueous concentration distributions with and without sorption retardation. The proposed framework provides improved insights into the influence of concentration-dependent nonlinear retardation of arsenic and contributes to an effective numerical methodology for predicting species migration patterns in heterogeneous groundwater systems.

2 Model Formulation

Consider a steady-state two-dimensional model of pollutant concentration in a heterogeneous aquifer. The contaminants, with concentration in the aqueous phase being $\mathscr{C}_{As}(x,y,t)$ $[ML^{-3}]$ and in the sorbed phase being $S(x,y,t)$ $[MM^{-1}]$, travel alongside water in the xy−plane at an angular trajectory. The present study is formulated with the following assumptions:

- Instantaneous exchange between aqueous and solid phase.
- Constant mean flow field.
- The contaminant transport is limited to two dimensions.
- Single contaminant system is considered.

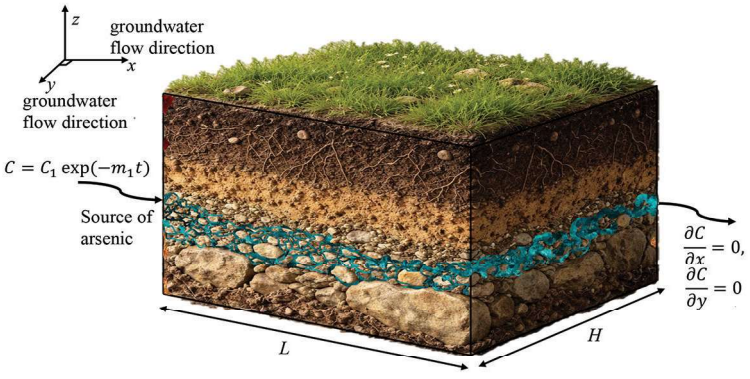

Figure 1: Physical layout of contaminant transport in groundwater system.

The governing equation for arsenic transportation in the groundwater system is the advection-dispersion equation (ADE) [21], given by:

$$R\frac{\partial \mathscr{C}_{\mathrm{As}}}{\partial t}=\frac{\partial}{\partial x}\left(\mathscr{D}_x(x)\,\frac{\partial \mathscr{C}_{\mathrm{As}}}{\partial x}\right)+\frac{\partial}{\partial y}\left(\mathscr{D}_y(y)\,\frac{\partial \mathscr{C}_{\mathrm{As}}}{\partial y}\right)-u\frac{\partial \mathscr{C}_{\mathrm{As}}}{\partial x}-v\frac{\partial \mathscr{C}_{\mathrm{As}}}{\partial y}. \tag{1}$$

In Eq. (1), the spatially-dependent hydrodynamic dispersion coefficients are denoted by $\mathscr{D}_x(x)$ $[L^2T^{-1}]$ and $\mathscr{D}_y(y)$ $[L^2T^{-1}]$ along the direction of contaminant flow, respectively. u $[LT^{-1}]$ and v $[LT^{-1}]$ are the seepage velocities of groundwater along the x– and the y– direction, respectively. This term defines the advection mechanism of contaminant transport.

R is the retardation factor which arises from sorption of contaminants into the soil medium. Since sorption is dependent on material properties of the soil, R is a relation calibrating the effect of the soil properties (bulk density, ρ $[ML^{-3}]$ and porosity, ϕ), the concentration $\mathscr{C}_{\mathrm{As}}$, and the sorbed concentration S. This relation is:

$$R=1+\frac{\rho}{\phi}\frac{\partial S}{\partial \mathscr{C}_{\mathrm{As}}}. \tag{2}$$

The sorption models employed for the study, along with their respective retardation factors for arsenic transport, are as in Table 1.

To introduce heterogeneity in the system, an asymptotical function of the hydrodynamic dispersion coefficients is considered as defined in Eq. (3)

$$\mathscr{D}_x(x)=D_x\frac{x}{x+b}\,; \qquad \mathscr{D}_y(y)=D_y\frac{y}{y+b}, \tag{3}$$

where, b $[L]$ is the asymptotic parameter. The variation of the dispersion ratio along the direction of flow is attenuated in the soil medium as b increases. Therefore, introducing heterogeneity into the aquifer medium.

Incorporating Eq. (3) in Eq. (1), the obtained equation is:

$$R\frac{\partial \mathscr{C}_{\mathrm{As}}}{\partial t}=D_x\frac{x}{x+b}\frac{\partial^2 \mathscr{C}_{\mathrm{As}}}{\partial x^2}+D_y\frac{y}{y+b}\frac{\partial^2 \mathscr{C}_{\mathrm{As}}}{\partial y^2}-\left[u-D_x\frac{b}{(x+b)^2}\right]\frac{\partial \mathscr{C}_{\mathrm{As}}}{\partial x}$$
$$-\left[v-D_y\frac{b}{(y+b)^2}\right]\frac{\partial \mathscr{C}_{\mathrm{As}}}{\partial y}. \tag{4}$$

To better investigate the effect of b on the system, Eq. (4) is subjected to a coordinate transformation:

$$X=x+b\,; \qquad Y=y+b. \tag{5}$$

The transformation is applied on Eq. (4) to obtain Eq. (6)

$$R\frac{\partial \mathscr{C}_{\mathrm{As}}}{\partial t}=D_x\left(1-\frac{b}{X}\right)\frac{\partial^2 \mathscr{C}_{\mathrm{As}}}{\partial X^2}+D_y\left(1-\frac{b}{Y}\right)\frac{\partial^2 \mathscr{C}_{\mathrm{As}}}{\partial Y^2}-\left[u-D_x\frac{b}{X^2}\right]\frac{\partial \mathscr{C}_{\mathrm{As}}}{\partial X}-\left[v-D_y\frac{b}{Y^2}\right]\frac{\partial \mathscr{C}_{\mathrm{As}}}{\partial Y}. \tag{6}$$

The analysis of the system is considered under the following conditions:

1. Initial condition:

$$\mathscr{C}_{\mathrm{As}}(X,Y,t)=\mathscr{C}_{(\mathrm{As})_\circ}\exp(m\,(X+Y)), \qquad 0<X<L, 0<Y<H, t=0. \tag{7}$$

Here, $\mathscr{C}_{As^\circ}$ is the initial concentration of arsenic contaminants in the system, and m is an arbitrary constant.

2. Boundary conditions:

- Dirichlet boundary condition at the inlet defined as:

$$\mathscr{C}_{As}(X,Y,t) = \mathscr{C}_{(As)_1} exp(-m_1 t), \qquad X = 0, 0 < Y < H, t > 0, \tag{8}$$

$$\mathscr{C}_{As}(X,Y,t) = \mathscr{C}_{(As)_2} exp(-m_2 t), \qquad Y = 0, 0 < X < L, t > 0, \tag{9}$$

with $\mathscr{C}_{As1}$ and $\mathscr{C}_{As2}$ as constant background contaminant concentration and m_1 and m_2 as arbitrary constants.

- Neumann boundary condition at the outlet defined by:

$$\frac{\partial \mathscr{C}_{As}}{\partial X} = 0, \qquad X = L, 0 < Y < H, t > 0, \tag{10}$$

$$\frac{\partial \mathscr{C}_{As}}{\partial Y} = 0, \qquad Y = H, 0 < X < L, t > 0. \tag{11}$$

The mathematical model and conditions are defined on the system in Eq. (6)-(11), and the retardation factor, R, is presented in Table 1, along with the parameter values reported in literature. The Henry, Freundlich, Langmuir and Tóth isotherm models are adopted with parameters from experimentally determined adsorption site studies [7], [22], [23]. The experimentally validated data points are widely used to characterise the interaction of arsenic species with the porous medium under different sorption mechanisms. Their systematic incorporation into the numerical model enables a physically meaningful comparison of the sorption models for arsenic plume evolution. For comparison purposes, a baseline case of unit retardation ($R = 1$) is considered. This represents the case where there is no sorption, and the transport of arsenic species is governed solely by advection and dispersion. This serves as a reference frame for evaluating linear and nonlinear sorption cases and their influence on plume evolution in the system.

Table 1: The different sorption isotherms and the value of the parameters used for the study of arsenic transport [7], [22].

Sorption Isotherm	Sorption Type	Sorption Equation	Retardation factor	Sorption Parameter	Symbol	Parameter Value
Henry	Linear	$S = k_d \mathscr{C}_{As}$	$R_1 = 1 + \frac{\rho}{\phi} k_d$	Henry coefficient	k_d	0.1358
Freundlich	Non-linear	$S = k_d \mathscr{C}_{As}{}^q$	$R_2 = 1 + \frac{\rho\, k_d\, q}{\phi} \mathscr{C}_{As}{}^{q-1}$	Freundlich coefficient Non-linearity parameter	k_d q	0.1358 0.5209

Lang-muir	Non-linear	$S = \frac{\alpha k_l \mathscr{C}_{As}}{1+\alpha \mathscr{C}_{As}}$	$R_3 = 1 + \frac{\rho}{\phi} \frac{\alpha\, k_l}{(1+\alpha \mathscr{C}_{As})^2}$	Langmuir coefficient Maximum sorption capacity	α k_l	0.15 0.07223
Tóth [23]	Non-linear	$S = \frac{k_T \mathscr{C}_{As}}{(a_T + C)^{1/t}}$	$R_4 = 1 + \frac{\rho}{\phi} \frac{k_T [a_T + \mathscr{C}_{As}(1-\frac{1}{t})]}{(a_T + \mathscr{C}_{As})^{1/t+1}}$	Maximum sorption capacity Tóth coefficient Hetero-geneity parameter	kT aT t	1.16 16.41 1.31

3 Numerical Discretization

A uniform discretisation of the physical layout is adopted to ensure numerical consistency when applying the proposed PR-ADI numerical scheme. The discretisation is also relevant to understanding the stability of the numerical scheme applied to the system.

3.1 ADI Numerical Scheme

The model accounts for heterogeneity via an asymptotic dispersion parameter and incorporates nonlinear sorption effects. The complexity of the resulting system precludes analytical treatment. Consequently, the equations are subjected to the ADI scheme. The method decomposes the two-dimensional problem into successive one-dimensional tridiagonal systems by alternating the implicit discretisation direction between the x– and y– directions, thereby reducing computational effort compared with a standard fully implicit Crank-Nicolson scheme. The PR-ADI scheme also ensures the solution is conditionally stable on the system when the CFL conditions are satisfied and is therefore applicable for handling complex heterogeneous systems [24].

Discretization along x– axis

A uniform computational grid is established for the spatial domain by dividing the two axes into uniform intervals, $\Delta X = \Delta Y$, such that $X_i = i\Delta X$ and $Y_j = j\Delta Y$. The temporal axis is uniformly discretised into the grids of intervals $t_n = n\Delta t$. A second order central difference scheme is applied for discretising the spatial derivative terms along the x– and y–directions. In the first half-step, the iteration is considered along the x–direction, and therefore the derivatives of x are evaluated at $(2n+1)^{th}$ time-level, whereas the derivatives of y are evaluated at the time-level 2n. Following the discretisation method, discretised version of Eq. (6) is as follows:

$$R_{i,j}^{2n}\frac{\mathscr{C}_{(As)_{i,j}}^{2n+1}-\mathscr{C}_{(As)_{i,j}}^{2n}}{\Delta t}=\quad D_x\left(1-\frac{b}{i\Delta X}\right)\left(\frac{\mathscr{C}_{(As)_{i+1,j}}^{2n+1}-2\mathscr{C}_{(As)_{i,j}}^{2n+1}+\mathscr{C}_{(As)_{i-1,j}}^{2n+1}}{\Delta X^2}\right)$$
$$+D_y\left(1-\frac{b}{j\Delta X}\right)\left(\frac{\mathscr{C}_{(As)_{i,j+1}}^{2n}-2\mathscr{C}_{(As)_{i,j}}^{2n}+\mathscr{C}_{(As)_{i,j-1}}^{2n}}{\Delta Y^2}\right)$$
$$-\left[u-D_x\frac{b}{(i\Delta X)^2}\right]\left(\frac{\mathscr{C}_{(As)_{i+1,j}}^{2n+1}-\mathscr{C}_{(As)_{i-1,j}}^{2n+1}}{2\Delta X}\right)$$
$$-\left[v-D_y\frac{b}{(j\Delta X)^2}\right]\left(\frac{\mathscr{C}_{(As)_{i,j+1}}^{2n}-\mathscr{C}_{(As)_{i,j-1}}^{2n}}{2\Delta Y}\right). \tag{12}$$

Re-arranging according to the time-levels, Eq. (12) becomes:

$$\left[\frac{r_1}{4}-\frac{r_3}{2}\right]\mathscr{C}_{(As)_{i+1,j}}^{2n+1}+\left[\frac{R_{i,j}^{2n}}{2}+r_3\right]\mathscr{C}_{(As)_{i,j}}^{2n+1}-\left[\frac{r_1}{4}+\frac{r_3}{2}\right]\mathscr{C}_{(As)_{i-1,j}}^{2n+1}$$
$$=-\left[\frac{r_2}{4}-\frac{r_4}{2}\right]\mathscr{C}_{(As)_{i,j+1}}^{2n}+\left[\frac{R_{i,j}^{2n}}{2}-r_4\right]\mathscr{C}_{(As)_{i,j}}^{2n}+\left[\frac{r_2}{4}+\frac{r_4}{2}\right]\mathscr{C}_{(As)_{i,j-1}}^{2n}, \tag{13}$$

with the coefficients defined as:

$$r_1=\left[u-D_x\frac{b}{(i\Delta X)^2}\right],\qquad r_3=D_x\left(1-\frac{b}{i\Delta X}\right),$$
$$r_2=\left[v-D_y\frac{b}{(j\Delta X)^2}\right],\qquad r_4=D_y\left(1-\frac{b}{j\Delta X}\right), \tag{14}$$

Discretization along y− axis

In the second half-step, the iteration in the *y*− directions results in evaluating the derivatives of y at the next time-level 2n+2, with derivatives of x still at time-level 2n+1. This iteration method leads to the discretised equation of Eq. (6):

$$R_{i,j}^{2n}\left(\frac{\mathscr{C}_{(As)_{i,j}}^{2n+2}-\mathscr{C}_{(As)_{i,j}}^{2n+1}}{\Lambda t}\right)=D_x\left(1-\frac{b}{i\Lambda X}\right)\left(\frac{\mathscr{C}_{(As)_{i+1,j}}^{2n+1}-2\mathscr{C}_{(As)_{i,j}}^{2n+1}+\mathscr{C}_{(As)_{i-1,j}}^{2n+1}}{\Lambda X^2}\right)$$
$$+D_y\left(1-\frac{b}{j\Delta X}\right)\left(\frac{\mathscr{C}_{(As)_{i,j+1}}^{2n+2}-2\mathscr{C}_{(As)_{i,j}}^{2n+2}+\mathscr{C}_{(As)_{i,j-1}}^{2n+2}}{\Delta Y^2}\right)$$
$$-\left[u-D_x\frac{b}{(i\Delta X)^2}\right]\left(\frac{\mathscr{C}_{(As)_{i+1,j}}^{2n+1}-\mathscr{C}_{(As)_{i-1,j}}^{2n+1}}{2\Delta X}\right)$$
$$-\left[v-D_y\frac{b}{(j\Delta X)^2}\right]\left(\frac{\mathscr{C}_{(As)_{i,j+1}}^{2n+2}-\mathscr{C}_{(As)_{i,j-1}}^{2n+2}}{2\Delta Y}\right). \tag{15}$$

Re-arranging it as an implicit equation in terms of the $(2n+2)^{th}$ time-level:

$$\left[\frac{r_2}{4}-\frac{r_4}{2}\right]\mathscr{C}_{(As)_{i,j+1}}^{2n+2}+\left[\frac{R_{i,j}^{2n}}{2}+r_4\right]\mathscr{C}_{(As)_{i,j}}^{2n+2}-\left[\frac{r_2}{4}+\frac{r_4}{2}\right]\mathscr{C}_{(As)_{i,j-1}}^{2n+2}$$
$$=-\left[\frac{r_1}{4}-\frac{r_3}{2}\right]\mathscr{C}_{(As)_{i+1,j}}^{2n+1}+\left[\frac{R_{i,j}^{2n}}{2}-r_3\right]\mathscr{C}_{(As)_{i,j}}^{2n+1}+\left[\frac{r_3}{4}+\frac{r_3}{2}\right]\mathscr{C}_{(As)_{i-1,j}}^{2n+1}. \tag{16}$$

Discretization of the Neumann boundary conditions Eq. (10)-(11) at the three time-steps are:

$$\mathscr{C}_{(\mathrm{As})_{\mathtt{i}+1,\mathtt{j}}^{2\mathtt{n}+1}} = \mathscr{C}_{(\mathrm{As})_{\mathtt{i}-1,\mathtt{j}}^{2\mathtt{n}+1}}, \qquad \text{at } \mathtt{i} = M, \quad 0 \le \mathtt{j} \le N, \quad \mathtt{n} \ge 0, \tag{17}$$

$$\mathscr{C}_{(\mathrm{As})_{\mathtt{i},\mathtt{j}+1}^{2\mathtt{n}}} = \mathscr{C}_{(\mathrm{As})_{\mathtt{i},\mathtt{j}-1}^{2\mathtt{n}}}. \qquad \text{at } \mathtt{j} = N, \quad 0 \le \mathtt{i} \le M, \quad \mathtt{n} \ge 0. \tag{18}$$

$$\mathscr{C}_{(\mathrm{As})_{\mathtt{i},\mathtt{j}+1}^{2\mathtt{n}+2}} = \mathscr{C}_{(\mathrm{As})_{\mathtt{i},\mathtt{j}-1}^{2\mathtt{n}+2}}. \qquad \text{at } \mathtt{j} = N, \quad 0 \le \mathtt{i} \le M, \quad \mathtt{n} \ge 0. \tag{19}$$

Applying the discretized boundary conditions Eq. (17) - (19), Eq. (12) is reduced to:

$$-r_3\mathscr{C}_{(\mathrm{As})_{\mathtt{i}-1,\mathtt{j}}^{2\mathtt{n}+1}} + \left[\frac{R_{\mathtt{i},\mathtt{j}}^{2\mathtt{n}}}{2} + r_3\right]\mathscr{C}_{(\mathrm{As})_{\mathtt{i},\mathtt{j}}^{2\mathtt{n}+1}} = -\left[\frac{r_2}{4} - \frac{r_4}{2}\right]\mathscr{C}_{(\mathrm{As})_{\mathtt{i},\mathtt{j}+1}^{2\mathtt{n}}} + \left[\frac{R_{\mathtt{i},\mathtt{j}}^{2\mathtt{n}}}{2} - r_4\right]\mathscr{C}_{(\mathrm{As})_{\mathtt{i},\mathtt{j}}^{2\mathtt{n}}} + \left[\frac{r_2}{4} + \frac{r_4}{2}\right]\mathscr{C}_{(\mathrm{As})_{\mathtt{i},\mathtt{j}-1}^{2\mathtt{n}}}, \tag{20}$$

$$\left[\frac{r_1}{4} - \frac{r_3}{2}\right]\mathscr{C}_{(\mathrm{As})_{\mathtt{i}+1,\mathtt{j}}^{2\mathtt{n}+1}} + \left[\frac{R_{\mathtt{i},\mathtt{j}}^{2\mathtt{n}}}{2} + r_3\right]\mathscr{C}_{(\mathrm{As})_{\mathtt{i},\mathtt{j}}^{2\mathtt{n}+1}} - \left[\frac{r_1}{4} + \frac{r_3}{2}\right]\mathscr{C}_{(\mathrm{As})_{\mathtt{i}-1,\mathtt{j}}^{2\mathtt{n}+1}} = r_4\mathscr{C}_{(\mathrm{As})_{\mathtt{i},\mathtt{j}-1}^{2\mathtt{n}}} + \left[\frac{R_{\mathtt{i},\mathtt{j}}^{2\mathtt{n}}}{2} - r_4\right]\mathscr{C}_{(\mathrm{As})_{\mathtt{i},\mathtt{j}}^{2\mathtt{n}}}, \tag{21}$$

$$-r_3\mathscr{C}_{(\mathrm{As})_{\mathtt{i}-1,\mathtt{j}}^{2\mathtt{n}+1}} + \left[\frac{R_{\mathtt{i},\mathtt{j}}^{2\mathtt{n}}}{2} + r_3\right]\mathscr{C}_{(\mathrm{As})_{\mathtt{i},\mathtt{j}}^{2\mathtt{n}+1}} = r_4\mathscr{C}_{(\mathrm{As})_{\mathtt{i},\mathtt{j}+1}^{2\mathtt{n}}} + \left[\frac{R_{\mathtt{i},\mathtt{j}}^{2\mathtt{n}}}{2} - r_4\right]\mathscr{C}_{(\mathrm{As})_{\mathtt{i},\mathtt{j}}^{2\mathtt{n}}}. \tag{22}$$

The discretized boundary conditions Eq. (17) - (19) are then applied to Eq. (16) and is reduced to:

$$-r_4\mathscr{C}_{(\mathrm{As})_{\mathtt{i},\mathtt{j}-1}^{2\mathtt{n}+2}} + \left[\frac{R_{\mathtt{i},\mathtt{j}}^{2\mathtt{n}}}{2} + r_4\right]\mathscr{C}_{(\mathrm{As})_{\mathtt{i},\mathtt{j}}^{2\mathtt{n}+2}} = -\left[\frac{r_1}{4} - \frac{r_3}{2}\right]\mathscr{C}_{(\mathrm{As})_{\mathtt{i}+1,\mathtt{j}}^{2\mathtt{n}+1}} + \left[\frac{R_{\mathtt{i},\mathtt{j}}^{2\mathtt{n}}}{2} - r_3\right]\mathscr{C}_{(\mathrm{As})_{\mathtt{i},\mathtt{j}}^{2\mathtt{n}+1}} + \left[\frac{r_3}{4} + \frac{r_3}{2}\right]\mathscr{C}_{(\mathrm{As})_{\mathtt{i}-1,\mathtt{j}}^{2\mathtt{n}+1}}, \tag{23}$$

$$\left[\frac{r_2}{4} - \frac{r_4}{2}\right]\mathscr{C}_{(\mathrm{As})_{\mathtt{i},\mathtt{j}+1}^{2\mathtt{n}+2}} + \left[\frac{R_{\mathtt{i},\mathtt{j}}^{2\mathtt{n}}}{2} + r_4\right]\mathscr{C}_{(\mathrm{As})_{\mathtt{i},\mathtt{j}}^{2\mathtt{n}+2}} - \left[\frac{r_2}{4} + \frac{r_4}{2}\right]\mathscr{C}_{(\mathrm{As})_{\mathtt{i},\mathtt{j}-1}^{2\mathtt{n}+2}} = r_3\mathscr{C}_{(\mathrm{As})_{\mathtt{i}-1,\mathtt{j}}^{2\mathtt{n}+1}} + \left[\frac{R_{\mathtt{i},\mathtt{j}}^{2\mathtt{n}}}{2} - r_3\right]\mathscr{C}_{(\mathrm{As})_{\mathtt{i},\mathtt{j}}^{2\mathtt{n}+1}}, \tag{24}$$

$$-r_4\mathscr{C}_{(\mathrm{As})_{\mathtt{i},\mathtt{j}-1}^{2\mathtt{n}+2}} + \left[\frac{R_{\mathtt{i},\mathtt{j}}^{2\mathtt{n}}}{2} + r_4\right]\mathscr{C}_{(\mathrm{As})_{\mathtt{i},\mathtt{j}}^{2\mathtt{n}+2}} = r_3\mathscr{C}_{(\mathrm{As})_{\mathtt{i}-1,\mathtt{j}}^{2\mathtt{n}+1}} + \left[\frac{R_{\mathtt{i},\mathtt{j}}^{2\mathtt{n}}}{2} - r_3\right]\mathscr{C}_{(\mathrm{As})_{\mathtt{i},\mathtt{j}}^{2\mathtt{n}+1}}. \tag{25}$$

The above system of equations form a tridiagonal matrix solved using Thomas algorithm under the boundary condition and the initial condition defined in Eq. (7) and Eq. (8)-(11).

4 Results and Discussion

The model considers the numerical solution of an unsteady two-dimensional convective–dispersive transport equation with an added source term. Sorption effects are incorporated through four sorption isotherm formulations (as in Table 1). The governing equation is solved using the Alternating Direction Implicit (ADI) scheme proposed by Peaceman and Rachford. An exponential initial concentration distribution is prescribed, while Dirichlet and Neumann boundary conditions are imposed at the inlet and outlet boundaries, respectively. The resulting discretization leads to a system of tridiagonal algebraic equations, which is efficiently solved using the classical Thomas algorithm. The input parameters used for the initial simulations are listed below.

$M = 60$, $N = 60$, $P = 10000$, $L = 2$ km, $H = 2$ km, $\mathscr{C}_{\circ} = 50$ mg/L, $\mathscr{C}_1 = \mathscr{C}_2 = 45$ mg/L, $D_x = D_y = 1\times10^{-3}$ g/m^2, $u = v = 1\times10^{-4}$ m/d, $\rho = 2.65$ mg/L, $\phi = 0.13$, $m = 2$, $m_1 = m_2 = 1$, $b = 0.6$ km.

Table 2: Variation of sorbed concentration and retardation factor with aqueous arsenic concentration for different sorption isotherms.

Isotherm	Parameter	Concentration (mg/L)				
		5	10	20	30	45
Henry	R_1	3.768	3.768	3.768	3.768	3.768
	S_1	0.679	1.358	2.716	4.074	6.111
Freundlich	R_2	1.67	1.48	1.34	1.28	1.23
	S_2	v0.314	0.451	0.647	0.799	0.986
Langmuir	R_3	1.07	1.04	1.01	1.01	1.00
	S_3	0.082	0.157	0.287	0.397	0.535
Tóth	R_4	2.87	2.38	1.88	1.64	1.45
	S_4	0.559	0.953	1.492	1.859	2.252

Figure 2 refers to the effect of space-dependent sorption isotherm-caused retention of arsenic as opposed to a system with constant retardation (R = 1). Different sorption isotherms not only delay arsenic transport but also reshape plume evolution by introducing concentration-dependent retardation effects that alter tailing behaviour and core migration.

Henry isotherm, as in Figure 2a, is a linear sorption termwhich is linear with concentration and the corresponding retardation factor remains constant (R = 3.768) throughout the domain as recorded in Table 2, also being the largest retardation factor. The figure shows overlap across almost the entire domain, with the closest agreement with the baseline case among all the sorption models considered. Due to the visible overlap, the magnitude of a uniform retardation factor does not change the dominant mechanism of arsenic in the groundwater system but can delay the onset of the transport. It only scales the transport parameters of the species in the system to another distinct constant, and therefore, the plume shape is not altered. Arsenic remains advection-dispersion dominated. A constant retardation, or linear sorption term, does not change the plume evolution pattern as it does not account for the concentration of the species present in the system, and the availability of sorption sites for the species. The large retardation factor indicates that the addition of arsenic concentration will have a uniform level of retention in the groundwater system.

Figure 2b shows the retention effect of the Freundlich isotherm, which is an extension of the Henry isotherm to represent a non-linear sorption term, against the baseline retardation (R = 1). Since the isotherm is concentration-dependent, Table 2 notes decreasing retardation factor with increasing concentration. In higher-concentration regions, a significant amount of arsenic is adsorbed onto the soil matrix, reducing the mobility of the species down the domain and clearly distinguishing it from the baseline contour at 30 mg/L. But at lower concentrations, the Freundlich contours are closer to the baseline case, especially at 10 mg/L. This implies that the retardation is not uniform throughout the domain. As arsenic migrates downstream, the species that is retention-dominated in higher-concentration regions becomes advection-dominated and moves at a greater velocity across the domain, diminishing the separation. Therefore, regions of high concentration readily adsorb arsenic,

while those at lower concentrations do not, thereby altering the plume shape. The plume fringe is separated greatly near the core of the domain. So, Freundlich sorption preferentially retards the plume tail, leading to enhanced attenuation at the margins while the core advances more freely. This is characteristic as Freundlich often predicts longer tailing in breakthrough curves.

In Figure 2c, the transport of arsenic under the Langmuir sorption is indicated, compared to baseline retardation. The Langmuir sorption accounts for concentration dependence as well as the sorption-site capacity of the soil matrix and therefore shows a nonuniform profile of arsenic migration. It also indicates a secondary flow of arsenic concentration at the source due to the perpendicular flow of arsenic into the domain and variations of velocity experienced at different concentration levels [25]. This trend is observed at high concentration, and the retention due to the Langmuir isotherm is stronger than the unit retardation for the same. The effect of retention weakens downstream because the isotherm accounts for soil saturation. In high-concentration regions, the retardation is clearly distinguished from the baseline, but the sorption sites are saturated. Additional arsenic, when added, has no available sorption sites and must travel downstream, as evidenced by the low retardation factor in Table 2 at higher concentrations. As they travel downstream, readily available sorption sites attenuate the arsenic species, thereby reducing their mobility. This is observed in the figure, where the inward contour level is at 10 mg/L. Contaminants can be retained only until the soil reaches saturation. This explains the weakened effect of the isotherm on the retardation of arsenic into the core of the domain.

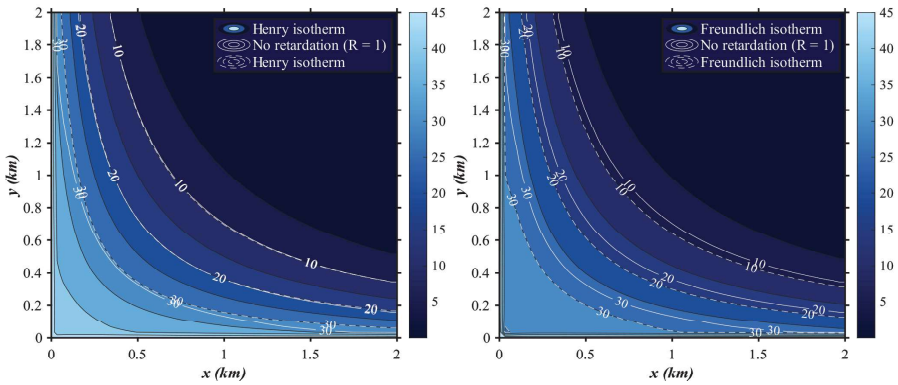

(a) Henry sorption term

(b) Freundlich sorption term

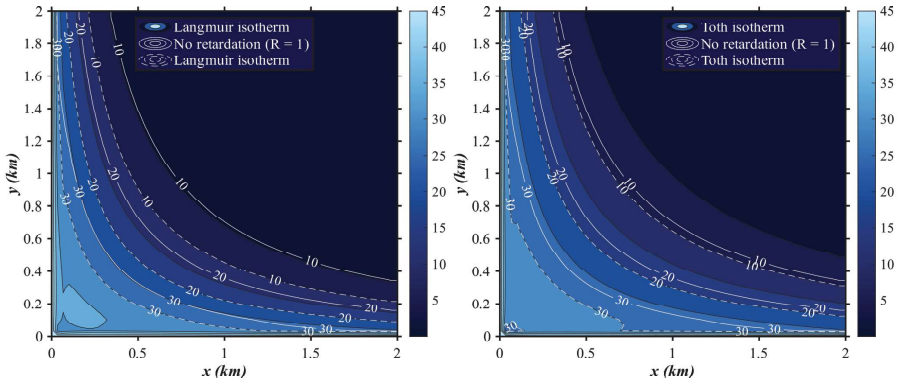

(c) Langmuir sorption term (d) Tóth sorption term

Figure 2: Arsenic transport under the influence of linear and different nonlinear sorption models with the contour levels representing arsenic transport with $R = 1$.

Tóth isotherm, given by Figure 2d shows smooth and intermediate deviations of contours as opposed to the contour lines of baseline retardation ($R = 1$). Neither an excessive trailing nor an early breakthrough curve is observed. This leads to the inference that the retardation transitions smoothly between the lower- and higher-concentration regimes. The contour plot shows a sustained retention near the source, as well as preserving retardation as it migrates downstream in the heterogeneous aquifer. The migration pattern suggests that this nonlinear sorption balances the adsorption between Langmuir and Freundlich sorption, providing a more realistic arsenic retention pattern in the groundwater systems. While the total sorbed arsenic is increasing with an increase in concentration (as in Table 2) the increment in adsorption capacity decreases gradually as seen in the gradual decrease of the retardation factor recorded. The sustained retardation observed across the domain shows accurate retention at the source with an inward contour line of 30 mg/L (compared to Figure 2b) and also promotes attenuation of the species downstream, as seen by the inward while also not shifting significantly (compared to Figure 2c). The isotherm captures the heterogeneity of the system, including delayed contaminant breakthrough and continuous plume attenuation into the soil matrix.

Table 3: Porosity of different soil textures with a range of Al and Fe content found according to case studies.

Soil type	Porosity	Al (*wt* %)	Fe (*wt* %)
Gravel	0.3	0.3-1.0	0.1 - 0.5
Coarse	0.35	1.0 - 3.0	0.3 - 1.5
Fine sand	0.40	2.0 -5.0	0.8 - 2.5
Silt	0.33	4.0 - 8.0	1.5 - 4.0
Clay	0.17	6.0-12.0	3.0-6.0

Table 4: Retardation factor for various sorption models of arsenic concentrations $\mathscr{C}_{As}$ = 20.0 *mg/L* and $\mathscr{C}_{As}$ = 30.0 *mg/L*. The values are iterated for varying soil textures and illustrate the influence of soil porosity on arsenic retention across the sorption models.

Porosity	$\mathscr{C}_{As}$ =20.0 *mg/L*				$\mathscr{C}_{As}$ =30.0 *mg/L*			
	R_1	R_2	R_3	R_4	R_1	R_2	R_3	R_4
0.3	2.195	1.1482	1.0016	8.4340	2.1950	1.1220	1.0007	8.2412
0.35	2.0243	1.1270	1.0013	7.3720	2.0243	1.1046	1.0006	7.2067
0.4	1.8963	1.1111	1.0011	6.5755	1.89628	1.0915	1.0005	6.4309
0.33	2.0864	1.1347	1.0014	7.7582	2.0864	1.1109	1.0006	7.5829
0.17	3.1089	1.2615	1.0027	14.1189	3.1089	1.2153	1.0012	13.7786

The comparison with conservative tracer case $R = 1$ reveals that nonlinear sorption isotherms introduce spatially variable retardation, with the Freundlich model exhibiting preferential tailing, while the Tóth isotherm provides a smoother and more physically representative transition with source-zone saturation effects along with the tailing effect.

As a consistency check for the numerical error, the Freundlich isotherm is implemented at the limiting case of $q = 1$. This reduces algebraically to the linear Henry isotherm. The modified concentration profile from the Freundlich model was coded independently for Henry concentration fields spatially and temporally. The $L-2$ error norm was observed to be on the order of 10^{-6}, consistent with the isotherms and confirming the implementation. The present study is not calibrated against a field study, but the obtained numerical solution has been confirmed through existing literature (in [20] and the stability analysis with a modified von Neumann analysis (as in [24]).

The retention of arsenic in soil pertains to the minerology of the soil with higher attenuation for textures with higher Al/Fe content [26], [27]. The soil porosity and Al/Fe content for soil types are presented in Table 3 to identify the effect of soil type on retention isotherm behaviour. An exact number for the Al/Fe content is not appropriate for a general study, as it depends on the geology and the type of aquifer; a fitting range of values is provided.

Table 4 provides the retardation factors for each sorption isotherm model, with values for aqueous arsenic concentration in soil matrices of varying porosity. A decrease in the model's porosity reflects a consistent increase in arsenic retardation in the system. This enhances the arsenic retention patterns in finer-grained soils. Concentration-independent attenuation is observed under the Henry sorption model, indicating that retention is governed solely by soil properties. Alternatively, simulations under the Freundlich model show a mild concentration dependence, with slightly reduced retention at higher concentrations. Nonlinear behaviour is observed in the Langmuir model, which yields values close to unity at lower concentrations, highlighting the effect of soil saturation. Tóth isotherm produces the highest retardation values and reflects the effects of both soil texture as well as concentration of arsenic present in the medium. This result emphasises that the attenuation strength of arsenic in the soil matrix is influenced by soil texture, without altering the qualitative transport behaviour.

The presence of aluminium(*Al*) and iron(*Fe*) oxides in the aquifer materials plays a crucial role in governing arsenic transport, along with other mineralogical properties. Table 3 shows that finer-grained soils, such as clay and silt, have higher contents of *Al* and *Fe* as compared to coarse soils such as gravel and coarse sand. This can be attributed to fine soil having a greater surface area for arsenic sorption from groundwater flow, thereby enhancing attenuation of the contaminant in a low-porosity medium. In comparison, coarser soils are characterised by higher porosity, which facilitates greater arsenic mobility, and by limited adsorption capacity. The numerical model result is consistent with mineral surface availability and established geochemical controls [28], [29].

5 Conclusion

In this study, a numerical scheme was employed to analyse the retention pattern of arsenic contaminants in the soil medium of different soil textures. The evolution of arsenic plumes in groundwater was recorded for different retardation factors, consistent with their respective sorption models. The major findings from the research can be summarised as:

- Attenuation of arsenic contaminants in soil medium is strongly influenced by the sorption model employed for the study, along with the soil texture and mineral properties.
- Linear sorption (Henry model) showed a concentration-independent and uniform retardation pattern, whereas the nonlinear sorptions introduced a spatial variance to the retention pattern of arsenic, affecting the plume shape and tailing as compared to unit retardation.
- The soil texture showed that arsenic mobility is greater for coarse-grained soil that has poor Al/Fe content, whereas finer soils retain more arsenic on the soil surface.

The results confirm that arsenic transport in the groundwater system is governed by soil characteristics and isotherm types, along with advective-dispersive mechanisms captured by the numerical model.

6 Future Scope

Future studies could explore the coupling of arsenic sorption and desorption under reactive transport conditions. Multi-contaminant interactions can also be explored to incorporate further complex aquifers. Additionally, coupling numerical simulations with machine learning approaches could enhance predictive modelling of arsenic migration and retention in diverse hydrogeological settings.

Credit authorship contribution statement

Aiswarya R Iyer: Writing – original draft, Visualization, Software, Methodology, Investigation, Conceptualization.

Smita S Nagouda: Writing – review & editing, Investigation, Supervision, Methodology.

Declaration of competing interest

The authors declare that they have no known competing interests.

Acknowledgements

Dr S N Smita would like to thank CHRIST University for supporting this work through the SEED Money grant number **CU-ORS-SM-24/26**.

Data Availability

No data was used for the research described in the article.

References

[1] Juárez-Aparicio F., Morales-Arredondo J. I., and Hernández M. A. A., "Simultaneous removal of fluoride and arsenic from drinking groundwater using limestones from bajío guanajuatense, mexico", *Arab. J. Geosci.*, vol. 17, (109), 2024. doi: 10.1007/s12517-024-11896-6.

[2] Júnez-Ferreira H. E., Bautista-Capetillo J., and Robles-Rovelo C. O., "Aqueous arsenic speciation with hydrogeochemical modeling and correlation with fluorine in groundwater in a semiarid region of mexico", *Water*, vol. 14, p. 519, 2022. doi: 10.3390/w14040519.

[3] Yu X., LeMonte J. J., and Li J., "Hydrologic control on arsenic cycling at the groundwater–surface water interface", *Environ. Sci. Technol.*, vol. 57, (1), pp. 222–230, 2023. doi: 10.1021/acs.est.2c05930.

[4] Cao F., Kleja D. B., Tiberg C., and Jarsjö J., "Large-scale arsenic mobilization from legacy sources in anoxic aquifers: Multiple methods and multi-decadal perspectives", *Sci. Total Environ.*, vol. 892, p. 164 565, 2023. doi: 10.1016/j.scitotenv.2023.164565.

[5] Ziegler M. A., Ng G.-H. C., and Cozzarelli I. M., "Arsenic in petroleum-contaminated groundwater near bemidji, minnesota is predicted to persist for centuries", *Water*, vol. 13, (11), p. 1485, 2021. doi: 10.3390/w13111485.

[6] Atteia O, Prommer H, Vlassopoulos D, André L., and Cohen G, "Muflowreact: A library to solve multiphase multicomponent reactive transport on unstructured meshes", *Groundwater*, vol. 62, (3), pp. 357–370, 2024. doi: 10.1111/gwat.13345.

[7] Acharya A. et al., "Adsorption of arsenic and fluoride: Modeling of single and competitive adsorption systems", *Heliyon*, vol. 10, (11), 2024. doi: 10.1016/j.heliyon.2024.e31967.

[8] Amrutha, Jeppu G., Girish C., Prabhu B., and Mayer K., "Multi-component adsorption isotherms: Reviewand modeling studies", *Environmental processes*, vol. 10, (2), p. 38, 2023. doi: 10.1007/s40710-023-00631-0.

[9] Deng X., Huang Y., and Guo Z., "Reactive migration mechanism of fe2+ and as3+ during groundwater discharge into river water: Insights from sand column experiments", *J. Hydrol.*, vol. 625, p. 130 033, 2023. doi: 10.1016/j.jhydrol.2023.130033.

[10] Petrosino F., "Spatial distribution and source identification of arsenic using reactive transport modeling", *Sci. Total Environ.*, vol. 898, p. 165 468, 2023. doi: 10.1016/j.scitotenv.2023.165468.

[11] Nghiem A. A., Prommer H., and Mozumder M. R. H., "Sulfate reduction accelerates groundwater arsenic contamination even in aquifers with abundant iron oxides", *Nat. Water*, vol. 1, pp. 151–165, 2023. doi: 10.1038/s44221-022-00022-z.

[12] Wang Z., Wang Q., and Guo Y., "Seawater–groundwater interaction governs trace metal zonation in a coastal sandy aquifer", *Water Resour. Res.*, vol. 59, (9), 2023. doi: 10.1029/2022WR032828.

[13] Onwudiwe D. C., Seheri N. H., and Kgabi N. A., "Functionalized graphitic carbon nitride as adsorbent for the removal of arsenic and lead from groundwater", *Discov. Water*, vol. 4, (38), 2024. doi: 10.1007/s43832-024-00095-9.

[14] Sun Y., Yu F., and Han C., "Research progress on adsorption of arsenic from water by modified biochar and its mechanism: A review", *Water*, vol. 14, p. 1691, 2022. doi: 10.3390/w14111691.

[15] Boruah T., Tyagi N., Gupta S. K., Chabukdhara M., and Malik T., "Understanding the adsorption of iron oxide nanomaterials in magnetite and bimetallic form for the removal of arsenic from water", *Front. Environ. Sci.*, vol. 11, p. 1 104 320, 2023. doi: 10.3389/fenvs.2023.1104320.

[16] Shah J. R., Akhtar M. S., and Alshehri F., "Modeling the transport of inorganic arsenic species through field soils: Irrigation and soil structure effect", *Water*, vol. 16, p. 386, 2024. doi: 10.3390/w16030386.

[17] Letechipia R. O., González-Trinidad J., and Júnez-Ferreira H., "Aqueous arsenic speciation and hydrogeochemical modeling in a semiarid region", *Water*, vol. 14, p. 519, 2022. doi: 10.3390/w14040519.

[18] Xu Z., Serata R., and Wainwright H., "Reactive transport modeling for supporting climate resilience at groundwater contamination sites", *Hydrol. Earth Syst. Sci.*, vol. 26, pp. 755–773, 2022. doi: 10.5194/hess-26-755-2022.

[19] Al-Hashimi O. et al., "A comprehensive review for groundwater contamination and remediation: Occurrence, migration and adsorption modelling", *Molecules*, vol. 26, (19), p. 5913, 2021. doi: 10.3390/molecules26195913.

[20] Radha R., Singh R. K., and Singh M. K., "Contaminant transport analysis under non-linear sorption in a heterogeneous groundwater system", *Applied Mathematics in Science and Engineering*, vol. 30, (1), pp. 736–761, 2022.

[21] Ding X.-H., Luo B., Zhou H.-T., and Chen Y.-H., "Generalized solutions for advection–dispersion transport equations subject to time-and space-dependent internal and boundary sources", *Computers and Geotechnics*, vol. 178, p. 106 944, 2025. doi: 10.1016/j.compgeo.2024.106944.

[22] Hafeznezami S. et al., "Adsorption and desorption of arsenate on sandy sediments from contaminated and uncontaminated saturated zones: Kinetic and equilibrium modeling", *Environmental Pollution*, vol. 215, pp. 290–301, 2016. doi:10.1016/j.envpol.2016.05.029.

[23] Davis M. G., Yan K., and Murphy J. G., "Evaluating adsorption isotherm models for determining the partitioning of ammonium between soil and soil pore water in environmental soil samples", *Biogeosciences*, vol. 21, (23), pp. 5381–5392, 2024. doi: 10.5194/bg-21-5381-2024.

[24] Aiswarya R. I. and Smita S. N., "Directional injection-driven contaminants transport in groundwater system with asymptotically varying dispersion coefficients", *Journal of Contaminant Hydrology*, p. 104 813, 2025. doi: 10.1016/j.jconhyd.2025.104813.

[25] Siddheshwar P., Narayana M., Saha R., and Nagouda S. S., "A comparative study of thermoconvective flows of a newtonian fluid over three horizontal undulated surfaces in a porous medium", *Journal of Heat Transfer*, vol. 144, (9), p. 092 701, 2022. doi: 10.1115/1.4054803.

[26] Guo M., Shi L., Gu W., and Wu W., "Adsorption and its mechanism of arsenate in aqueous solutions by red soil", *Water*, vol. 14, (4), p. 579, 2022. doi: 10.3390/w14040579.

[27] Chi Z., Xie X., Pi K., and Wang Y., "Mineralogical controls on arsenite adsorption onto soils: Batch experiments and model-based quantification", *Science of the Total Environment*, vol. 767, p. 144 920, 2021. doi: 10.1016/j.scitotenv.2020.144920.

[28] Boruah P., Gogoi B., and KarakN., "Recent advances in iron oxide-based nanomaterials for arsenic removal from water: A review", *Frontiers in Environmental Science*, vol. 11, p. 1 104 320, 2023. doi: 10.3389/fenvs.2023.1104320.

[29] Sharma R. K., Solanki K., Dixit R., Sharma S., and Dutta S., "Nanoengineered iron oxide-based sorbents for separation of various water pollutants: Current status, opportunities and future outlook", *Environmental Science: Water Research & Technology*, vol. 7, (5), pp. 818–860, 2021. doi: 10.1039/D1EW00108F.